

Comparative study of the phonons in non-superconducting BaC₆ and superconducting CaC₆ using inelastic x-ray scattering

A. C. Walters,^{1,2,*} C. A. Howard,² M. H. Upton,^{3,4} M. P. M. Dean,⁴ A. Alatas,³ B. M. Leu,³ M. Ellerby,² D. F. McMorrow,² J. P. Hill,⁴ M. Calandra,⁵ and F. Mauri⁵

¹*ESRF, Polygone Scientifique Louis Néel, 6 rue Jules Horowitz, 38000 Grenoble, France*

²*London Centre for Nanotechnology and Department of Physics and Astronomy, University College London, London WC1E 6BT, United Kingdom*

³*Advanced Photon Source, Argonne National Laboratory, Argonne, IL 60439, USA*

⁴*Condensed Matter Physics and Materials Science Department, Brookhaven National Laboratory, Upton, New York 11973*

⁵*Université Pierre et Marie Curie, 4 Place Jussieu-case postale 115, 72252 Paris, CEDEX 05, France*

(Dated: August 24, 2021)

The low energy phonons of two different graphite intercalation compounds (GICs) have been measured as a function of temperature using inelastic x-ray scattering (IXS). In the case of the non-superconductor BaC₆, the phonons observed are significantly higher (up to 20%) in energy than those predicted by theory, in contrast to the reasonable agreement found in superconducting CaC₆. Additional IXS intensity is observed below 15 meV in both BaC₆ and CaC₆. It has been previously suggested that this additional inelastic intensity may arise from defect or vacancy modes not predicted by theory (d'Astuto et al, Phys. Rev. B **81** 104519 (2010)). Here it is shown that this additional intensity can arise directly from the polycrystalline nature of the available samples. Our results show that future theoretical work is required to understand the relationship between the crystal structure, the phonons and the superconductivity in GICs.

PACS numbers: 71.20.Tx,63.20.kd,74.25.Kc,63.20.kg,78.70.Ck

Keywords: graphite intercalates, superconductivity, electron-phonon coupling, inelastic x-ray scattering

I. INTRODUCTION

Since the discovery of superconductivity in YbC₆ ($T_c = 6.5$ K) and CaC₆ ($T_c = 11.5$ K) at temperatures over an order of magnitude higher than previously found in graphite intercalation compounds (GICs)^{1,2}, the properties of this family of GICs have been extensively studied by a variety of different experimental techniques³⁻⁸. Although initially an exotic superconducting mechanism was proposed involving acoustic plasmons⁹, subsequent density functional theory (DFT) studies described the superconductivity via a more orthodox electron-phonon (e-ph) coupling mechanism with s-wave symmetry¹⁰⁻¹³. These DFT descriptions predict that the e-ph coupling is approximately equal for phonons associated with vibration of the carbon atoms and for phonons associated with movement of the intercalant calcium.

At present there are experimental studies in the literature which give conflicting viewpoints concerning the nature of the e-ph coupling in GICs. A large Ca isotope effect ($\alpha(\text{Ca}) \sim 0.5$) has been measured in CaC₆⁶, which, if viewed within the BCS description of superconductivity, suggests that only the phonons due to the vibration of calcium are involved in the electron pairing. In contrast, angle-resolved photoemission spectroscopy (ARPES) measurements on CaC₆⁸ have found that the e-ph coupling to graphite-like high-energy phonons is so strong that it can explain the superconducting transition temperature alone, without any additional coupling to calcium phonons. These discrepancies point to the need for a detailed study of the phonons in GICs, to both

test the DFT description and to look for direct evidence for e-ph coupling involving specific phonons. Moreover, phonon studies in graphitic systems in general are important as the electron-phonon interactions in these systems are under much scrutiny¹⁴⁻¹⁶.

Superconductivity in GICs is directly linked to the graphite layer separation, with the superconducting transition temperature T_c increasing as the graphite layer separation d is reduced. This trend is supported both by the observed values of T_c in a variety of GICs⁵ and by measurements of T_c as a function of pressure in CaC₆¹⁷ and YbC₆¹⁸. Indeed in BaC₆ the graphite layer separation is so large that superconductivity appears to be suppressed entirely, with no superconducting transition observed down to 0.080 K¹⁹. It is therefore instructive to study the superconductivity in GICs by studying GICs with different intercalants, since by changing the intercalant one changes d and therefore tunes T_c .

In this paper we present the low energy phonon dispersions in non-superconducting BaC₆ and superconducting CaC₆ as measured using inelastic x-ray scattering (IXS). These data represent the first momentum-resolved phonon measurements on BaC₆. We find a substantial discrepancy between experiment and theory in the phonon energies of BaC₆, in contrast to the good agreement in the case of CaC₆. Like many other layered materials, GICs are difficult to synthesise as high-quality single crystals. We demonstrate here that the details of the preferred orientation (texture) of the crystallites in these GIC samples can lead to the observation of phonons which, because of their polarization, are theoretically for-

bidden to be observed. Our work highlights the importance of accounting for these effects in phonon studies of textured polycrystalline samples and calls for the need for single crystal GIC samples to address the role of the electron-phonon coupling in these materials.

The low energy phonons in CaC_6 have been measured previously²⁰ and found to be in good overall agreement with the published DFT calculations. Subsequent to this work two momentum-resolved phonon studies have been made on CaC_6 , an inelastic neutron scattering (INS) study, which concentrates primarily on the high energy graphite-like phonon modes²¹, and a study of the low energy phonons in CaC_6 performed using both IXS and INS²². While in Ref.²¹ good agreement was found with the calculated DFT phonon dispersions by taking account of the polycrystalline nature of the sample, in Ref.²² it was suggested that an additional phonon mode exists in CaC_6 of uncertain origin. Here we propose an alternative explanation: that the additional IXS intensity arises from the weak crystallographic texture in the polycrystalline GIC samples.

II. EXPERIMENTAL METHODS

The GIC samples were made using ZYA grade highly orientated pyrolytic graphite (HOPG) platelets purchased from GE Advanced Ceramics. The BaC_6 sample was made using the vapour transport method²³. An HOPG platelet was outgassed at 500°C and then sealed into a quartz tube along with the barium metal (purity $> 99.99\%$) under high vacuum ($< 10^{-6}$ mbar). The tube was then heated to 490°C and maintained at this temperature for 4 weeks. The CaC_6 samples used were prepared by immersing a HOPG platelet in a Li-Ca alloy for 10 days, as described elsewhere²⁴. CaC_6 samples made from the same batch were found to have a sharp superconducting transition at 11.5 K from magnetic susceptibility measurements. The very high purity of the samples ($> 99\%$ pure in both cases) can be seen in the $(00l)$ diffraction shown in Figure 1 (e) and 1 (f), where there are no visible Bragg peaks from any impurities.

The starting graphite (HOPG) is composed of small crystallites ($\approx 1 \mu\text{m}$) which have a strong preferred orientation (strong texture) perpendicular to the graphene planes (out-of-plane), giving a $(00l)$ mosaic with full-width half-maximum (FWHM) as low as 0.2° . However within the graphene planes (in-plane), the crystallites are orientated randomly²³. After intercalation the crystallites are still oriented randomly in-plane, but out-of-plane the orientation of the crystallites is more random, with the GICs studied here having $(00l)$ mosaics of 5° . This means that the texture is weaker in the GIC samples than in HOPG, since a weaker texture means that the samples are more like a perfect powders, which have zero texture.

CaC_6 has the structure $R\bar{3}m$, which can be described using a rhombohedral or a hexagonal basis². The calcium atoms are arranged in three different ways in dif-

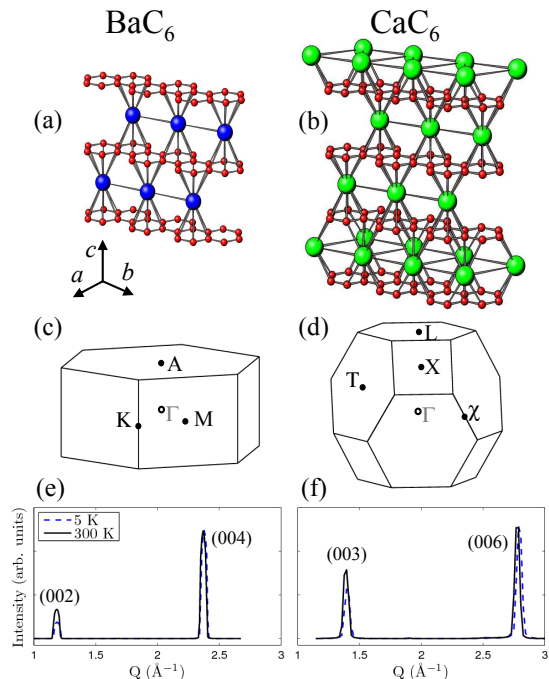


FIG. 1: The structural properties of BaC_6 and CaC_6 : (a)-(b) Crystal structure, (c)-(d) First Brillouin zone with symmetry points, (e)-(f) Diffraction on BaC_6 and CaC_6 measured in $(00l)$ direction at 5 K (dashed blue line) and at 300 K (solid black line) at 3-ID. The symmetry points shown are at the edge of the Brillouin zone apart from the Γ point, which is at the zone centre. There is practically no signal from impurities in the $(00l)$ diffraction from either sample.

ferent intercalant layers (called $A\alpha A\beta A\gamma$ stacking, where the Roman letters define graphite layers and the Greek letters intercalant layers). The unit cell of CaC_6 in the hexagonal basis is shown in Figure 1(b), and the shape of the first Brillouin zone is shown in Figure 1(d). Here we define the reciprocal lattice directions using the hexagonal basis, meaning that the out-of-plane direction is the $(00l)$ direction. This convention aids comparison with the BaC_6 data, as BaC_6 has the space group $P6_3/mmc$, which is normally described within the hexagonal basis. The stacking in BaC_6 is $A\alpha A\beta$, as shown in Figure 1(a). The first Brillouin zone of BaC_6 is presented in Figure 1(c). The lattice parameters of CaC_6 are $a = 4.333(2) \text{ \AA}$ and $c = 13.572(2) \text{ \AA}$ ²⁵, giving a graphite layer separation d of $4.524(1) \text{ \AA}$, and in BaC_6 the lattice parameters are $a = 4.302(6) \text{ \AA}$ and $c = 10.50(4) \text{ \AA}$ with $d = 5.25(2) \text{ \AA}$ ²⁶.

The IXS measurements were performed at 3-ID at the Advanced Photon Source, Argonne National Laboratory, with an incident x-ray energy of 21.657 keV ²⁷, providing an energy resolution between 2.2 and 2.4 meV, depending on the specific analyzer. The spectrometer has four analyzers, allowing energy scans to be done at different momentum transfers simultaneously. The momentum resolution in all cases was 0.072 \AA^{-1} in the scattering plane and 0.183 \AA^{-1} perpendicular to it. The phonon peaks

were fitted with pseudo-Voigt functions, which were appropriately scaled by the Bose factor. The phonon dispersions were produced by plotting the peak positions as a function of the phonon wavevector \mathbf{q} , defined within the equation $\mathbf{Q} = \mathbf{G} + \mathbf{q}$, where \mathbf{G} is the nearest reciprocal lattice vector and \mathbf{Q} the momentum transfer.

In order to model the effect of the crystallographic texture in the GIC samples on the phonon spectra, simulations of the IXS data were produced by summing hundreds of simulated IXS intensities, each of which was performed at a specific momentum transfer. The crystallographic texture was described by performing simulations over a volume in reciprocal space expressed in spherical polar coordinates $(|\mathbf{Q}|, \theta, \phi)$, where θ has its rotation axis out-of-plane. For the 2D powder simulations, the momentum transfers were selected using Lorentzian sampling of ϕ with a FWHM of 5° and allowing θ to take any value. For the 3D powder simulations both ϕ and θ were allowed to take any value. The summed IXS spectra were then convolved with the momentum and energy resolution of the IXS spectrometer. This method was also used in our recent INS study of CaC_6 ²¹.

The two-dimensionality of these GICs, together with the significant difference in mass between the intercalant and carbon, means that the phonon modes can be separated, to a good approximation, into four groups: I_{xy} , I_z , C_{xy} and C_z , where I_{xy} describes phonon modes purely due to vibrations of intercalant atoms in-plane, I_z the intercalant phonons out-of-plane, and $C_{xy(z)}$ the equivalent carbon in-plane (out-of-plane) phonons.

III. INELASTIC X-RAY SCATTERING MEASUREMENTS

A. Phonons in BaC_6

The $(00l)$ phonon dispersions of BaC_6 measured at both 5 K and 300 K are plotted in Figure 2, together with calculated dispersions¹¹. The measured Ba_z phonon branches are significantly higher in energy than the theoretical values: near the edge of the Brillouin zone, at symmetry point A, the measured phonon energy for the optic Ba_z mode is almost 20% larger than that predicted. In addition, in all of the measured IXS energy scans on BaC_6 there is additional intensity observed below 10 meV, plotted with full symbols, which is not predicted by theory.

So what is the origin of this discrepancy between experiment and theory in BaC_6 ? We consider a number of possibilities. The DFT calculations were performed using a different structure to the structure experimentally determined, which may have affected their results. In addition, the charge transfer from the Ba atoms to the graphene planes may be inaccurately predicted by theory. Finally, the calculations do not account for the polycrystallinity of the real samples, so part of the disagreement may be due to their crystallographic texture.

The published calculations for BaC_6 use lattice param-

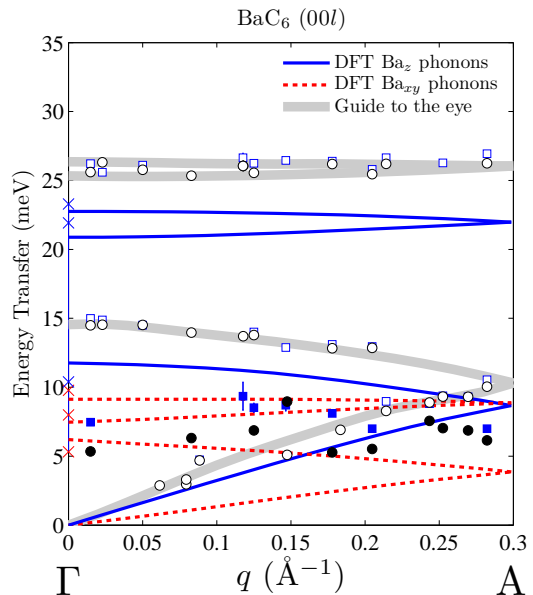


FIG. 2: BaC_6 $(00l)$ phonon dispersion measured at 5 K (squares) and 300 K (circles). Empty symbols denote Ba_z phonon intensity, full symbols label Ba_{xy} phonon intensity. The Ba_{xy} phonons should not be visible in this scattering geometry (see text). The theoretical dispersion of the Ba_z and Ba_{xy} phonons are plotted with solid lines and dashed lines respectively¹¹. A guide to the eye is plotted showing the dispersion of the Ba_z phonons at 300 K (thick solid line). The symmetry point A is located at $q = 0.299 \text{ \AA}^{-1}$. The crosses mark the phonon energies calculated at Γ using the experimental lattice parameters and space group of BaC_6 .

eters equivalent to $a = 4.350 \text{ \AA}$ and $c = 10.40 \text{ \AA}$ ¹¹ which are significantly different to the values found via x-ray diffraction ($a = 4.302(6) \text{ \AA}$ and $c = 10.50(4) \text{ \AA}$)²⁶. In addition, the space group of CaC_6 ($R\bar{3}m$) is used for BaC_6 in the calculation, rather than the experimentally found $P6_3/mmc$. To determine whether the observed discrepancy arises because of these structural differences, we performed an additional phonon calculation at the Γ point using the experimental structure and lattice parameters, as shown in Figure 2 (crosses). This calculation gives phonon energies in approximate agreement with the previous calculation, showing that the calculations are largely insensitive to small changes in both the lattice parameters and the space group. Therefore the incorrect structure used in the initial calculations can be eliminated as a cause of the discrepancies.

Another possibility is that the charge transfer from the Ba atoms to the graphite has been underestimated theoretically. If there is less charge than predicted in the graphitic π^* bands, then the bonds should be stronger than predicted, since filling the anti-bonding π^* band destabilizes the bonds. Stronger bonds lead directly to higher phonon energies. The effect of charge transfer on phonons in GICs has been predicted theoretically²⁸ and observed using Raman scattering¹⁶. This would explain

why the phonons are higher in energy than predicted, but cannot explain why additional intensity is observed below 10 meV.

The additional phonon intensity can be explained as a result of the crystallographic texture of the GIC samples. Here we argue that this signal arises from the excitation of I_{xy} phonons over a large volume in reciprocal space due to the weak crystallographic texture. For an ideal single crystal, and perfect instrumental resolution, the I_{xy} phonons are disallowed (their intensity is zero) when \mathbf{Q} is completely out-of-plane due to the $\mathbf{Q} \cdot \mathbf{e}(\mathbf{q})$ term in the IXS phonon cross-section, where $\mathbf{e}(\mathbf{q})$ is the eigenvector of the phonon with wavevector \mathbf{q} ²⁹. However in the case of the polycrystalline GIC samples studied, the weak crystallographic texture provides an explanation for the observation of the I_{xy} phonons. Even if the nominal momentum \mathbf{Q} is entirely out-of-plane, the large reciprocal space volume integrated over in each measurement due to the weak preferred orientation of the crystallites will include many values of \mathbf{Q} which have a significant component in-plane. This effect is discussed further in Section IV.

B. Phonons in CaC_6

Figure 3 presents the $(00l)$ phonon dispersion in CaC_6 at 5 K, 50 K and 300 K. A subset of the CaC_6 data has already been published²⁰, but the scope of the data presented here is much more extensive. The additional phonon intensity below 15 meV again results from the large mosaic of the sample and is discussed at length in Section IV. The phonon dispersions calculated using DFT are plotted on the same figure¹⁰. The two Ca_z modes are well described by the DFT calculations over the whole Q range sampled, especially in the case of the acoustic Ca_z mode. The higher energy mode which disperses between 30 and 40 meV (the optic Ca_z mode) is about 2 meV higher in energy than predicted, but the character of the dispersion is reasonably well described.

In both CaC_6 and BaC_6 the energies of the I_z modes are slightly hardened (< 1 meV) upon cooling from 300 K to 5 K, but there is no observable difference in CaC_6 between the data measured above and below T_c . The small temperature dependence most likely results from the reduction in the c lattice parameter upon cooling, visible in the diffraction presented in Figure 1(e) and 1(f).

IV. MODELLING THE CRYSTALLOGRAPHIC TEXTURE IN BaC_6 AND CaC_6

In Figures 4 and 5 a selection of phonon spectra measured at 300 K in the $(00l)$ direction in BaC_6 and CaC_6 are presented. In both cases two phonons are observed in the raw IXS data (the acoustic and optic I_z branches), as well as additional IXS intensity at low energies. In each of the panels two IXS simulations are plotted. The

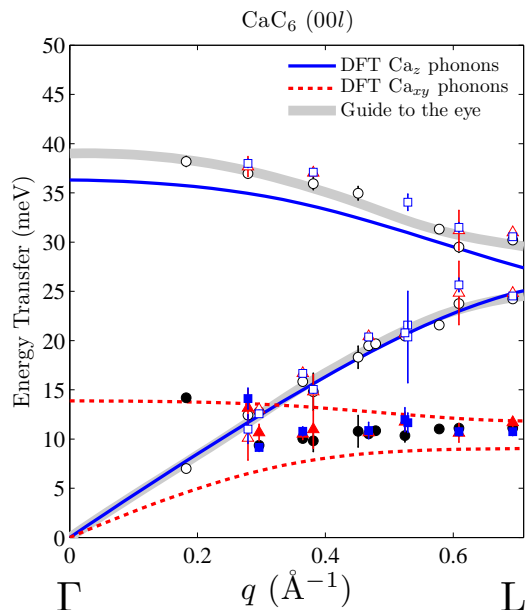


FIG. 3: CaC_6 $(00l)$ phonon dispersion measured at 5 K (squares), 50 K (triangles) and 300 K (circles). Empty symbols denote Ca_z phonon intensity, full symbols label Ca_{xy} phonon intensity. The Ca_{xy} phonons should not be visible in this scattering geometry (see text). The theoretical dispersion of the Ca_z and Ca_{xy} phonons are plotted with solid lines and dashed lines respectively¹⁰. A guide to the eye is plotted showing the dispersion of the experimental Ca_z phonons at 300 K (thick solid line). The symmetry point L is located at $q = 0.694 \text{ \AA}^{-1}$.

first simulation models the sample as a 2D powder: that is, the crystallites have no preferred orientation in-plane, but have a Lorentzian mosaic of $\text{FWHM} = 5^\circ$ out-of-plane, consistent with our x-ray diffraction. The second simulation models the sample with no preferred orientation (no texture): i.e. as a 3D powder. Both simulations are added to the experimental elastic intensity.

In the case of BaC_6 , plotted in Figure 4, the overall agreement is better with the 2D powder model than with the 3D powder model, especially in the ratio between the acoustic and optic Ba_z phonons. However in the 2D powder model the IXS intensity due to the Ba_{xy} phonons is much smaller than measured. The additional features predicted by the 3D powder model are similar to those observed, but there the intensities of the Ba_z phonons are underestimated. These observations suggest that perhaps the crystallographic texture of the BaC_6 samples is weaker than expected from our x-ray diffraction, lying somewhere between the 2D and 3D powder models.

In the CaC_6 data in Figure 5, the low energy IXS features look qualitatively similar to the Ca_{xy} features predicted by the 3D powder model. However the 3D powder description of CaC_6 is once again not a satisfactory description, as the intensity of the Ca_z phonons is underestimated in most cases and the IXS intensity at low energies is significantly overestimated³⁰. The measured

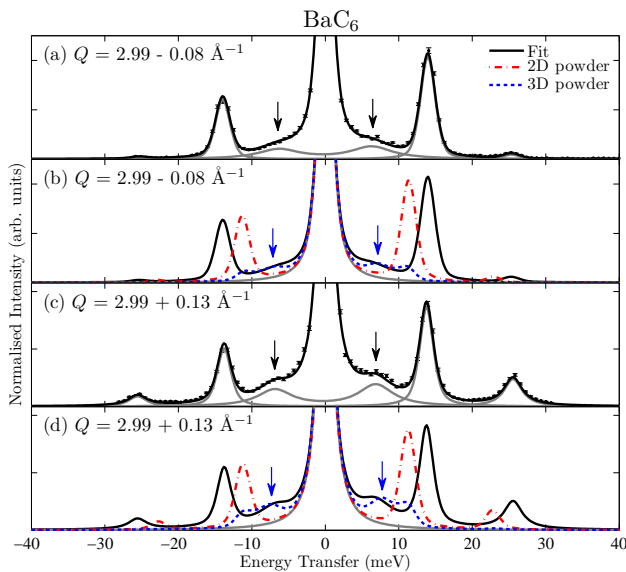


FIG. 4: (a) $(00l)$ IXS data at $Q = 2.91 \text{ \AA}^{-1}$ on BaC_6 at 300 K, plotted with the data fit and the decomposed fitted phonon peaks. (b) Fit to the data at $Q = 2.91 \text{ \AA}^{-1}$, plotted with the fitted elastic line and against IXS simulations based on *ab-initio* calculations¹¹ which use the 2D powder model and the 3D powder model described in the text. (c) & (d) Identical to (a) & (b) but for $Q = 3.12 \text{ \AA}^{-1}$. In each panel the experimental (simulated) IXS intensity due to Ba_{xy} phonons is marked with black (blue) arrows.

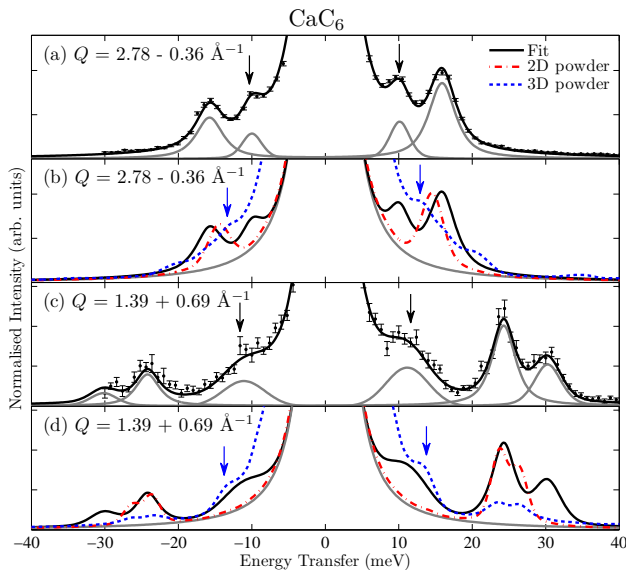


FIG. 5: (a) $(00l)$ IXS data at $Q = 2.42 \text{ \AA}^{-1}$ on CaC_6 at 300 K, plotted with the data fit and the decomposed fitted phonon peaks. (b) Fit to the data at $Q = 2.42 \text{ \AA}^{-1}$, plotted with the fitted elastic line and against IXS simulations based on *ab-initio* calculations¹⁰ which use the 2D powder model and the 3D powder model described in the text. (c) & (d) Identical to (a) & (b) but for $Q = 2.08 \text{ \AA}^{-1}$. In each panel the experimental (simulated) IXS intensity due to Ca_{xy} phonons is marked with black (blue) arrows.

CaC_6 data appear to lie somewhere between the 2D and 3D powder simulations, similar to the BaC_6 data, though the CaC_6 appears to be more like the 3D powder than BaC_6 . This suggests that the distribution of intercalant atoms in CaC_6 is rather random, which is consistent with the behavior of CaC_6 under pressure as studied with x-ray diffraction, where the Ca atoms are found to be very mobile⁴. More theoretical and experimental work is required in order to understand the complicated crystallographic texture of GICs, with more extensive x-ray diffraction being a natural starting point.

A recent IXS and INS study by d'Astuto et al.²² on CaC_6 suggested that the additional inelastic intensity was due to an interaction with the acoustic Ca_z mode, causing an avoided crossing, or anti-crossing, which is seen as a splitting in the acoustic Ca_z mode. Their work was supplemented by INS data, which allowed them to more easily access momenta nearer to the Γ point. The study concluded that the additional inelastic intensity could be due to a defect or vacancy mode. Although we cannot exclude this hypothesis, our simulations suggest that if the orientation of the crystallites in these samples is more random than previously thought, the weak crystallographic texture can account for the anomalous features without recourse to such a mode.

V. CONCLUSIONS

To summarise, the dispersions of the low-energy phonons in BaC_6 and CaC_6 have been measured as a function of temperature using inelastic x-ray scattering. In BaC_6 the experimental and DFT-calculated phonon dispersions¹¹ disagree, with measured phonon energies up to 20% higher than predicted. We suggest that this large discrepancy may result from an underestimation of the charge transfer from the Ba atoms to the graphite sheets in the theory. Our work motivates further study on BaC_6 in order to examine the underlying reasons for this disagreement. In contrast, reasonable agreement with theory is found in CaC_6 for the Ca_z phonons. This consistency between theory and experiment provides indirect supporting evidence for the DFT description¹⁰ of the superconductivity in CaC_6 .

No signatures of electron-phonon coupling are observed in the phonon dispersions or the phonon widths in either non-superconducting BaC_6 or superconducting CaC_6 , despite the drastically different superconducting transitions of these related compounds. In both BaC_6 and CaC_6 there is a small ($< 1 \text{ meV}$) hardening of the I_z phonons as the temperature is decreased, but this is likely due to a reduction in the c lattice parameter and is unaffected by the presence of superconductivity in CaC_6 below 11.5 K. The largest source of phonon broadening experimentally is very likely the weak crystallographic texture inherent in the GIC samples.

Finally, the IXS simulations presented here show that weak crystallographic texture in polycrystalline GIC

samples may lead to additional inelastic intensity from I_{xy} phonons. Such additional intensity has been observed recently in CaC_6 ^{20,22} and YbC_6 ³¹, but also in older INS studies on RbC_{24} ³² and KC_{24} ³³. This work provides a timely reminder that the crystallographic texture inherent in many graphitic systems may give rise to unexpected experimental effects.

Acknowledgments

We would like to thank Matteo d'Astuto and Michael Krisch for illuminating discussions. A. C. W. would like

to thank Ian Wood and Richard Thanki for their assistance and the EPSRC and STFC for funding. Calculations were performed at the IDRIS supercomputing center (project 081202). The work at Brookhaven is supported in part by the US DOE under contract No. DEAC02-98CH10886 and in part by the Center for Emergent Superconductivity, an Energy Frontier Research Center funded by the US DOE, Office of Basic Energy Sciences. The work at the Advanced Photon Source was supported by the US DOE, Office of Basic Energy Sciences, under contract No. DE-AC02-06CH11357.

-
- * Electronic address: andrew.walters@esrf.fr
- ¹ T. E. Weller, M. Ellerby, S. S. Saxena, R. P. Smith and N. T. Skipper, *Nature Physics* **1**, 39 (2005).
 - ² N. Emery, C. Hérold, M. d'Astuto, V. Garcia, Ch. Bellin, J. F. Maréché, P. Lagrange, and G. Loupiau, *Physical Review Letters* **95**, 087003 (2005).
 - ³ R. Cubitt, J. S. White, M. Laver, M. R. Eskildsen, C. D. Dewhurst, D. McK. Paul, A. J. Crichton, M. Ellerby, C. Howard, Z. Kurban, and F. Norris, *Physical Review B* **75**, 140516(R) (2007).
 - ⁴ A. Gauzzi, N. Bendiab, M. d'Astuto, B. Canny, M. Calandra, F. Mauri, G. Loupiau, N. Emery, C. Hérold, P. Lagrange, M. Hanfland and M. Mezouar, *Physical Review B* **78**, 064506 (2008).
 - ⁵ J. S. Kim, L. Boeri, J. R. O'Brien, F. S. Razavi, and R. K. Kremer, *Physical Review Letters* **99**, 027001 (2007).
 - ⁶ D. G. Hinks, D. Rosenmann, H. Claus, M.S. Bailey and J. D. Jorgenson, *Physical Review B* **75**, 014509 (2007).
 - ⁷ R. S. Gonnelli, D. Daghero, D. Delaude, M. Tortello, G. A. Ummarino, V. A. Stepanov, J. S. Kim, R. K. Kremer, A. Sanna, G. Profeta, and S. Massidda, *Physical Review Letters* **100**, 207004 (2008).
 - ⁸ T. Valla, J. Camacho, Z-H. Pan, A. V. Fedorov, A. C. Walters, C. A. Howard and M. Ellerby, *Physical Review Letters* **102**, 107007 (2009).
 - ⁹ G. Csányi, P. B. Littlewood, A. H. Nevidomskyy, C. J. Pickard and B. D. Simons, *Nature Physics* **1**, 42 (2005).
 - ¹⁰ M. Calandra and F. Mauri, *Physical Review Letters* **95**, 237002 (2005).
 - ¹¹ M. Calandra and F. Mauri, *Physical Review B* **74**, 094507 (2006).
 - ¹² A. Sanna, G. Profeta, A. Floris, A. Marini, E. K. U. Gross and S. Massidda, *Physical Review B* **75**, 020511 (2007).
 - ¹³ M. Calandra, G. Profeta, F. Mauri, *Physical Review B* **82**, 165111 (2010).
 - ¹⁴ S. Pisana, M. Lazzeri, C. Casiraghi, K. S. Novoselov, A. K. Geim, A. C. Ferrari, and F. Mauri, *Nature Materials* **6**, 198 (2007).
 - ¹⁵ M. Lazzeri and F. Mauri, *Physical Review Letters* **97**, 266407 (2006).
 - ¹⁶ M. P. M. Dean, C. A. Howard, S. S. Saxena and M. Ellerby, *Physical Review B* **81**, 045405 (2010).
 - ¹⁷ A. Gauzzi, S. Takashima, N. Takeshita, C. Terakura, H. Takagi, N. Emery, C. Hérold, P. Lagrange and G. Loupiau, *Physical Review Letters* **98**, 067002 (2007).
 - ¹⁸ R. P. Smith, A. Kusmartseva, Y. T. C. Ko, S. S. Saxena, A. Akrap, L. Forr, M. Laad, T. E. Weller, M. Ellerby, and N. T. Skipper, *Physical Review B* **74**, 024505 (2006).
 - ¹⁹ S. Nakamae, A. Gauzzi, F. Ladieu, D. L'Hôte, N. Eméry, C. Hérold, J.F. Maréché, P. Lagrange, G. Loupiau, *Solid State Communications* **145**, 493 (2008).
 - ²⁰ M. H. Upton, A. C. Walters, C. A. Howard, K. C. Rahnajat, M. Ellerby, J. P. Hill, D. F. McMorrow, A. Alatas, B. M. Leu and W. Ku, *Physical Review B* **76**, 220501(R) (2007).
 - ²¹ M. P. M. Dean, A. C. Walters, C. A. Howard, T. E. Weller, M. Calandra, F. Mauri, M. Ellerby, S. S. Saxena, A. Ivanov and D. F. McMorrow, *Physical Review B* **82**, 014533 (2010).
 - ²² M. d'Astuto, M. Calandra, N. Bendiab, G. Loupiau, F. Mauri, S. Zhou, J. Graf, A. Lanzara, N. Emery, C. Hérold, P. Lagrange, D. Petitgrand, M. Hoesch, *Physical Review B* **81**, 104519 (2010).
 - ²³ M. S. Dresselhaus and G. Dresselhaus, *Advances in Physics* **51**, 1 (2002).
 - ²⁴ S. Pruvost, C. Hérold, A. Hérold, and P. Lagrange, *Carbon* **42**, 1825 (2004).
 - ²⁵ N. Emery, C. Hérold, P. Lagrange, *Journal of Solid State Chemistry* **178**, 2947 (2005).
 - ²⁶ D. Guerard, M. Chaabouni, P. Lagrange, M. El Makrini and A. Hérold, *Carbon* **18**, 257 (1980).
 - ²⁷ T. S. Toellner, A. Alatas, A. Said, D. Shu, W. Sturhahn and J. Zhao, *Journal of Synchrotron Radiation* **13**, 211 (2006).
 - ²⁸ L. Boeri, G. B. Bachelet, M. Giantomassi and O. K. Andersen, *Physical Review B* **76**, 064510 (2007).
 - ²⁹ E. Burkel, *Reports on Progress in Physics* **63**, 171 (2000).
 - ³⁰ The large IXS intensity at low energy transfer in the CaC_6 '3D powder' simulations arises from the low energy phonons predicted around the X point in the Brillouin zone (shown in Figure 1(d)), which are intense because the IXS cross-section is inversely proportional to energy transfer.
 - ³¹ M. H. Upton, T. R. Forrest, A. C. Walters, C. A. Howard, M. Ellerby, A. H. Said, D. F. McMorrow, *Physical Review B* **82**, 134515 (2010).
 - ³² S. Funahashi, T. Kondow and M. Iizumi, *Physica B* **120**, 305 (1983).
 - ³³ A. Magerl, H. Zabel, J. J. Rush, *Synthetic Metals* **7**, 339 (1983).